2021-1

In silico and in vitro screening for potential anticancer candidates targeting GPR120

Ajay Pal
Technological University Dublin, ajay.pal@tudublin.ie

James Curtin
TU Dublin, james.curtin@tudublin.ie

Gemma K. Kinsella
Technological University Dublin, gemma.kinsella@tudublin.ie

Recommended Citation

Pal, A., Curtin, J. & Kinsella, G. (2021) In silico and in vitro screening for potential anticancer candidates targeting GPR120, *Bioorg Med Chem Lett,* 2021 Jan 1;31:127672. doi: 10.1016/j.bmcl.2020.127672

Bioorg. Med. Chem. Lett. 31 (2021) 127672

Contents lists available at ScienceDirect

Bioorganic & Medicinal Chemistry Letters

journal homepage: www.elsevier.com/locate/bmcl

In silico and *in vitro* screening for potential anticancer candidates targeting GPR120

Ajay Pal [a,b,c], James F. Curtin [a,d], Gemma K. Kinsella [a,*,e]

[a] School of Food Science and Environmental Health, College of Sciences and Health, Technological University Dublin, Dublin D07 ADY7, Ireland
[b] Environmental Sustainability and Health Institute (ESHI), Grangegorman, Technological University Dublin, Dublin D07 H6K8, Ireland

ARTICLE INFO

Keywords:
Molecular docking
Virtual screening
GPCR GPR120
FFA4 receptor
Colorectal cancer

ABSTRACT

The G-protein coupled receptor - GPR120 has recently been implicated as a novel target for colorectal cancer (CRC) and other cancer managements. In this study, a homology model of GPR120S (short isoform) was generated to identify potential anti-cancer compounds targeting the GPR120 receptor using a combined *in silico* docking-based virtual screening (DBVS), structure–activity relationships (SAR) and *in vitro* screening approach. SPECS database of synthetic chemical compounds (~350,000) was screened using the developed GPR120S model to identify molecules binding to the orthosteric binding pocket followed by an AutoDock SMINA rigid-flexible docking protocol.

The best 13 hit molecules were then tested *in vitro* to evaluate their cytotoxic activity against SW480 – human CRC cell line expressing GPR120. The test compound **1** (3-(4-methylphenyl)-2-[(2-oxo-2-phenylethyl)sulfanyl]-5,6-dihydrospiro(benzo[h]quinazoline-5,1′-cyclopentane)-4(3H)-one) showed ~ 90% inhibitory effects on cell growth with micromolar affinities (IC_{50} = 23.21–26.69 μM). Finally, SAR analysis of compound **1** led to the identification of a more active compound from the SPECS database showing better efficacy during cell-based cytotoxicity assay –**5** (IC_{50} = 5.89–6.715 μM), while a significant reduction in cytotoxic effects of **5** was observed in GPR120-siRNA pre-treated SW480 cells.

The GPR120S homology model generated, and SAR analysis conducted by this work discovered a potential chemical scaffold, *dihydrospiro(benzo[h]quinazoline-5,1′-cyclopentane)-4(3H)-one*, which will aid future research on anti-cancer drug development for CRC management.

GPR120 is a member of the Class A Rhodopsin-like G-protein coupled receptor (GPCR) family and the free-fatty acid receptors (FFAR) sub-family and exists in two homologous human isoforms (a short isoform at 361 amino acids and a long isoform at 377 amino acids).[1,2] It is also known as Free Fatty Acid 4 receptor (FFA4) – as its endogenous ligands have been identified as poly-unsaturated long-chain free fatty acids (PUFFA).[3–5] GPR120 over-expression has been reported in colorectal cancer (CRC) cell lines, at approximately 2–3 folds higher occurrence than for normal colorectal cells.[6] In CRC, GPR120 overexpression has been correlated with enhanced protein expression of proangiogenic factors such as vascular endothelial growth factors (VEGF), cyclooxegenase-2, and interleukin-8, as well as enhanced chemotactic activity of tumour cells.[6] This increased activity has been characterised as GPR120-induced activation of the PI3K/Akt-NF-κB signalling pathway.[6] GPR120 has also been reported to augment chemoresistance in breast cancer treatment by cross-talk through the Akt/NF-κB pathway.[7] An extensive review by Senatorov and Moniri[8] outlines the regulating role of GPR120 in various human cancers such as breast cancer, osteocarcinoma, melanoma prostate cancer, lung cancer, pancreatic cancer, and CRC.[8]

Tumour cells are known to secrete pro-angiogenic factors[9,10] and over-expression of GPR120 in CRC cell lines might be further stimulating the development of tumour angiogenesis. As well, GPR120 agonism is reported to result in lower rate of cell proliferation and cell migration and increased rate of apoptosis in various cancer cell lines and animal models.[8] Most of the FDA approved anti-angiogenic drugs[10] are

* Corresponding author.
E-mail address: gemma.kinsella@tudublin.ie (G.K. Kinsella).
[c] ORCID ID: https://orcid.org/0000-0002-8641-1497.
[d] ORCID ID: https://orcid.org/0000-0002-9320-9254.
[e] ORCID ID: https://orcid.org/0000-0002-6329-5841.

https://doi.org/10.1016/j.bmcl.2020.127672
Received 20 June 2020; Received in revised form 30 October 2020; Accepted 1 November 2020
Available online 6 November 2020

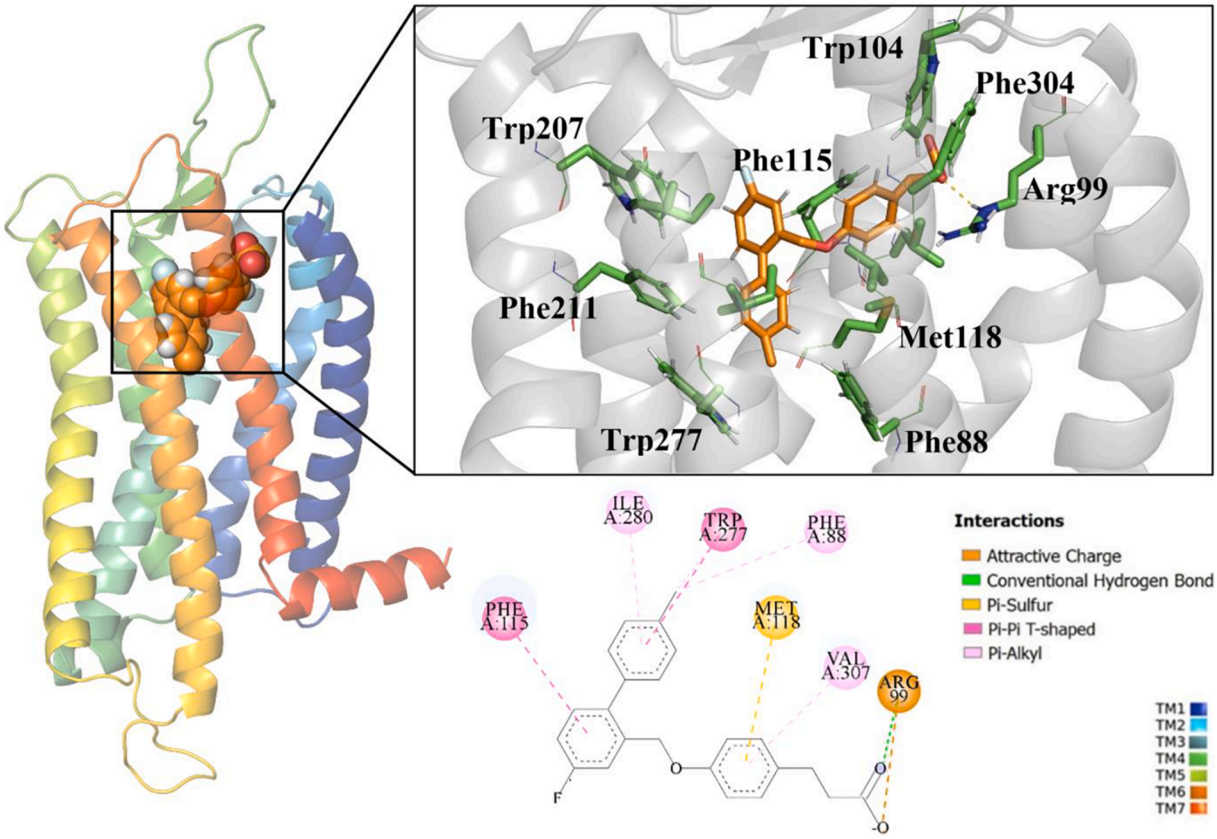

Fig. 1. Selected docked pose of TUG891 (binding score −9.87591) illustrating hydrogen bond interactions with Arg99 of GPR120S and a 2D interaction map of TUG891 in the orthosteric pocket binding pocket. The 3D images were visualized and rendered in PyMol v2.1.0.[21] The 2D interaction maps were generated in BIOVIA DS Client visualizer 2019.[22]

prescribed in combination with cytotoxic agents for effective CRC treatment. As GPR120 is involved at two extreme ends of the cancer therapeutics spectrum and tumour angiogenesis, it is of significant interest to develop and characterise small molecular anticancer agents targeting GPR120. Research studies, so far, have resulted in development of few potent GPR120 agonists only, such as TUG891 (see Fig 1), and a negative allosteric modulator, AH7614.[11]

Due to advances in protein engineering, the availability of GPCR crystallographic structures in the RCSB Protein Data Bank[12] has increased and allows the collection of structural data on GPCRs for early stage computer aided drug discovery (CADD). GPCRs crystal structure data can also be used as the reference templates for comparative modelling or homology modelling (HM), to predict the three dimensional (3D) structure of homologous GPCRs. Such *in silico* homology models of GPCRs have been successfully employed in virtual screening (VS) studies to identify lead molecules for developing therapeutic agents acting as agonists, inverse agonists, or antagonists.[13,14]. This methodology is termed structure-based virtual screening (SBVS) and more specifically docking-based virtual screening (DBVS) is the most applied in practice.[15,16].

In recent years, *in silico* VS studies followed by *in vitro* experiments have been successfully utilised to discover potential leads for developing GPCR ligands.[17] These *in silico* VS provide a faster and economical alternative to the wet-lab high-throughput screenings.[18] In addition to VS, analysis of structure–activity relationships (SARs) can lead to the design of potent and stable compounds by making rational structural modifications[19,20].

In this study, a GPR120 DBVS protocol was developed utilising molecular docking with an in-house homology model in iterative combination with an *in vitro* cytotoxicity screening assay and SAR analysis, resulting in the identification of novel compounds with anticancer potential and predicted to act through GPR120.

Methods

VS was performed on the Irish Centre for High-End Computing (ICHEC – www.ichec.ie) cluster. ICHEC provided CPU core units for computational processing and data storage space. The visual analysis and homology model building were carried out on an in-house 8 node (Intel® Core™ i7-4790 CPU @ 3.60 GHz × 8) Linux cluster. The visual analysis and image rendering was performed using PyMol Open-source version 2.1.0[21] and Biovia DS Client visualiser 2019.[22]

Homology modelling

The FASTA sequences of human GPR120 short isoform, termed GPR120S - (UniProt ID: Q5NUL3-2) was retrieved from the UniProt database (https://www.uniprot.org Uniprot 2016). The sequence was used for BLASTP analysis (https://blast.ncbi.nlm.nih.gov/Blast.cgi) run against the protein databank (PDB) to identify 3D determined protein structures according to the best multiple sequence alignment (MSA) score generated. The human Delta-like opioid receptor PDB-ID: 4N6H and human Orexin 2 receptor PDB-ID: 4S0V were used as template structures. Using the multiple sequence alignment of GPR120S and the templates, comparative 3D structural models were generated and validated using MODELLER (v9.14).[23] An in-house python pipeline (incorporating MODELLER) was developed using the KNIME platform (Konstanz Information Miner)[24] to automate the process from generation of 100 models using the MSA of selected templates to side-chain rotamer optimisation using SCWRL4[25] and evaluation of homology models by MODELLER's DOPE (Discrete Optimized Protein Energy) score function.[23] The models were ranked by the DOPE statistical

potential scoring models. The best models with the lowest DOPE values were then assessed for stereochemical properties using the MolProbity webserver[26] and their phi-psi Ramachandran plot were generated by using the PROCHECK online tool,[27] validation process (unpublished work).

Ligand library preparation

The SPECS database (www.specs.net) of synthetic chemical compounds (~350,000) was retrieved and processed in Biovia Discovery Studio's Pipeline Pilot v9.1 from Dassault Systèmes[22] to generate stereoisomers and tautomers, and remove compounds with molecular weight (greater than) > 650 and (less than) < 250 Dalton. The filtered chemical database was energy minimised using MMFF94 forcefield (steepest descent) in the open-source OpenBabel software package (http://openbabel.org/) and saved in sdf format.

Virtual screening and molecular docking

Molecular docking analysis was performed between the prepared ligands and the homology model of GPR120S (unpublished work) which was pre-processed in MGLs' AutoDock tools (www.autodock.scripps.edu)[28] to add polar hydrogens, charges by Kollman charge and assign torsion angles. The rigid-flexible docking protocol was followed by using Autodock SMINA (scoring and minimization in AutoDock VINA).[29] The binding site grid box was visually defined by employing AutoDock tools' Grid setting feature, based on the site-specific mutation study by Hudson et al. 2014[30] to include residues – Arg99(TM2), Trp104 (ECL1), Phe115 (TM3), Trp207, Phe211 (TM5), Trp277 (TM6) and Phe304 (TM7), deemed essential for ligand binding. The grid size dimensions were 40 × 60 × 60, with the (61.822, 59.75, 46.597) point set as the centre coordinates of the pocket. TUG891, being a selective potent agonist of GPR120,[31] was used as the reference ligand for docking analysis.

The docked poses generated by AutoDock SMINA were rescored with three different scoring functions, AutoDock Vina,[32] NNScore 2.0 (neural network based scoring function)[33] and DLSCORE (Deep learning based scoring function) https://github.com/sirimullalab/DLSCORE), to calculate the consensus binding affinity score (C_{score}) using Eq. (1). AutoDock VINA and SMINA predicts the binding affinities as Gibbs free energy (ΔG kCal/mol) while NNScore 2.0 and DLSCORE predicts the binding affinities as pK_d values[34].

$$C_{score} = V_{score} + S_{score} + (-NN_{score}) + (-DL_{score}) / Number\ of\ scoring\ functions \quad (1)$$

where: C_{score} is consensus docking score. V_{score} is docking using AutoDock Vina's default scoring function. S_{score} is docking score using SMINA's default scoring function. NN_{score} is docking score using NNScore 2.0 function. DL_{score} is docking score using DLScore function.

The ligands with a C_{score} lower than −9 were further analysed manually using the PyMol Open-source version 2.1.0[21] to enlist molecules for phase I of the *in vitro* screening based on their diverse scaffold chemistry. For phase II of *in vitro* screening, the chemical scaffold of the most cytotoxic test compound (from phase I) was used for a substructure search from the SPECS database docked pool using Discovery Studio's Pipeline Pilot from Dassault Systèmes 2017[22].

Cell culture and materials

SW480, a human CRC cell line was cultured in RPMI1640 growth media supplemented with 10% (v/v) Fetal Bovine Serum and incubated at 37 °C ± 1 °C in a humidified atmosphere with 5% CO_2. The cell culture media and reagents were procured from Sigma-Merck, unless otherwise mentioned. The test compounds for *in vitro* screening assays were procured from SPECS (www.specs.net). A stock solution of test compounds (20 mM) was prepared in 100% (w/v) DMSO and stored at −20 °C.

SW480 cells were transfected with 50 nM GPR120 (human) – 27mer siRNA duplex (SR317391) using siTran 2.0 siRNA transfection reagent (OriGene – www.origene.com) according to manufacturer's instructions after overnight seeding. Universal scrambled siRNA duplex (SR30004) was used as negative control in transfection experiments.

In vitro screening by cell-based cytotoxicity assay

Alamar blue based cytotoxicity assays were performed to determine inhibitory effects of the test compounds. SW480 cells were seeded at 10,000, 5,000 and 2500 cells per well in 96-well plates for 24, 48 and/or 72 h drug treatment, respectively. Required dilutions of test compounds were freshly prepared in 0.5% (v/v) DMSO growth media for cytotoxicity assays. After the treatment period, drug concentrations were replaced with 6% (v/v) alamar blue dye solution and the cells were incubated for 3 h under cell incubation conditions. Finally, the fluorescence signal was read using 560 nm excitation and 590 nm emission filters with Varioskan LUX Multimode Microplate Reader from ThermoFisher Scientific.

siRNA transfected cells were harvested after 24 h of transfection and used for cytotoxicity assays as explained above.

Statistical analysis

All data was presented as mean ± standard error of the mean (SEM). For the analysis and graphic representation of biological experimental IC_{50} values were calculated (GraphPad Prism 6 Software, La Jolla CA) using dose–response curves for the compounds. For plotting the dose–response curve, a non-linear regression curve fitting method was used where the mean positive control (50% DMSO in growth media) was defined as 0% and the mean vehicle control (0.5% DMSO in growth media) was defined 100%. For significance analysis, two-way analysis of variance (ANOVA) followed by Tukey's multiple comparison test was performed. $P < 0.05$ was considered statistically significant.

Results and discussion

Homology model of GPR120

The human GPR120S receptor model was developed using the MODELLER homology modelling tool.[23] The model which scored best (DOPE score −41156.738) as per the MODELLER scoring function was chosen as the final model and subjected to further energy minimization. The α-carbon RMSD (root mean squared deviation) between the templates 4N6H, 4S0V and the developed human GPR120S model is 1.386 Å and 0.652 Å, respectively. Poor rotamers and sidechain rotations, above the permitted range of 0.3%, were removed and replaced by SCWRL4 with the average sidechain rotamer from its backbone-dependent rotamer library based on kernel density estimates. The comparative analysis of the stereochemical parameters of the GPR120S model by Molprobity webserver showed high reliability of the generated models. The Ramachandran psi-phi evaluation showed that all helical amino acids are located in the region favouring a right-handed α-helix with no residues (0%) in a sterically disallowed region and 98–99% residues in the favoured regions. The GPR120S model was embedded in a lipid bilayer model and energy minimised (unpublished work).

Molecular docking of TUG891 to the GPR120S model

The docked pose of TUG891 – a potent GPR120 selective agonist, with the receptor binding pocket is shown in Fig 1. An arginine in TM2 (Arg99) is critical for interaction between the receptor and the -COOH group of its ligands by various studies.[30,31,35,36] Six other specific residues are essential for TUG891, and other GPR120 agonists binding and interaction which are: Trp104 (ECL1), Phe115 (TM3), Trp207, Phe211

Table 1
Virtual-HTS hit compounds from the SPECS database with scores from each scoring function and the consensus score (Cscore).

SPECS_ID	VINA	NNScore	DLScore	SMINA	Cscore
AN-970/40920574	−14.0799	10.6167	7.5808	−14.0822	−11.589
AK-968/41925665	−14.1500	8.4778	8.1736	−14.1543	−11.238
AO-299/41877474	−13.3325	9.3340	8.2664	−13.3348	−11.066
AE-848/32608035	−13.0308	9.5607	8.3752	−13.0307	−10.999
AN-970/40920575	−12.8216	9.9850	7.6430	−12.8253	−10.818
AG-690/40104520	−13.1039	8.8878	8.1416	−13.1031	−10.809
AJ-292/40857565	−13.1769	8.3250	8.0350	−13.1788	−10.678
AN-758/14707017	−12.5595	9.5580	7.3621	−12.5586	−10.509
AK-968/15252756	−12.5863	8.3809	8.2112	−12.5838	−10.441
AO-081/14456496	−11.7869	9.2246	7.7837	−12.2584	−10.263
AK-968/12713190	−12.3380	8.5407	7.6893	−12.3375	−10.226
AB-131/42301549	−12.2715	8.4730	6.8798	−12.8521	−10.119
AG-690/12137150	−12.2680	6.8487	7.0743	−12.2687	−9.614

(TM5), Trp277 (TM6) and Phe304 (TM7).[30] Interactions with these seven residues were selected as the main criterion for docked binding pose selection of TUG891.[30,31] Automated protein–ligand interaction analysis using the PLIP webserver[37] identified strong noncovalent interactions of residues forming contacts with TUG891 docked to the orthosteric binding pocket of GPR120S (Fig 1).

The selected docked pose for TUG891 (binding score −9.875) had interactions with Arg99 in all the predicted poses. The carboxylic acid of TUG891 forms a salt bridge (hydrogen bond and attractive charge interaction) with the Arg99 side-chain at a distance of 4.32 Å and a strong *T*-type (perpendicular) π-π stacking interaction between Phe115 and the second aromatic ring structure of TUG891. Other equitable hydrophobic and van der Waals interactions were also observed to stabilize the docked TUG891 in the orthosteric binding pocket.

In silico virtual screening

For virtual screening, the SPECS database (www.specs.net) containing ~ 350,000 commercially available well-characterised and drug-like molecules was screened against the GPR120S homology model. AutoDock SMINA was used as the molecular docking algorithm and the docked poses were rescored using an in-house consensus scoring function from Equation I (see methods). The best scoring poses docked into the receptor were manually evaluated by comparison with the docked pose of TUG891.

The docking-based virtual screening with a score cut off set at −9 (w.r.t binding score of TUG891 of −9.8) followed by a manual docking-pose analysis resulted in 13 compounds (Table 1) being selected for the first phase of *in vitro* screening through Alamar Blue cytotoxicity assay. As per the docking evaluation, these compounds are predicted to bind to the orthosteric binding pocket of GPR120S (see Fig 2) as well as having similar hydrophobic and / or electrostatic interactions with one or more of the residues reported essential for the pharmacological activity of the receptor.

The electrostatic potential surface maps shown in Fig 2 reveal that the GPR120S binding pocket is lined with negatively charged residues (red colour) which can interact with ligand molecules via hydrogen bond contacts, whereas the opening of the pocket is surrounded by neutral or weak potential residues. Theoretically ligands with a strong

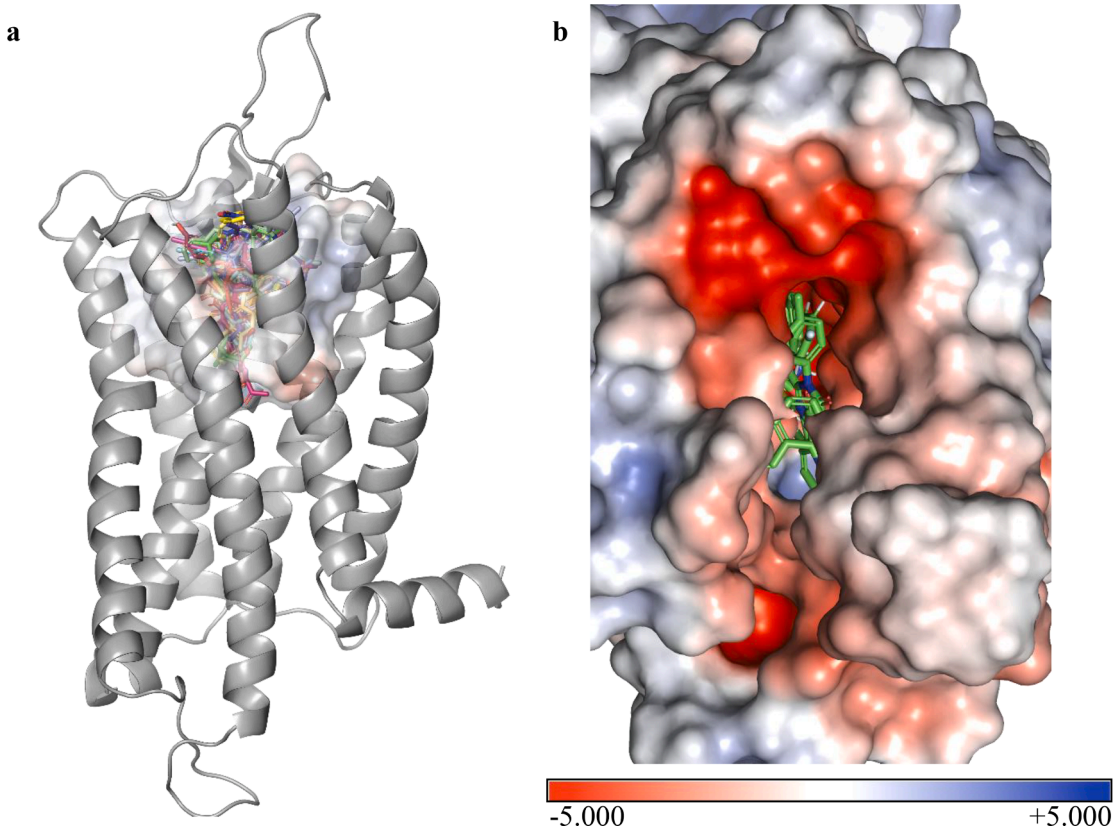

Fig. 2. Docking simulation of 13 test molecules with surface topology of the GPR120S orthosteric binding pocket (a). Zoomed in view of the electrostatic potential molecular surface of the orthosteric binding pocket as viewed from above (b) was calculated with APBS (Adaptive Poisson-Boltzmann Solver) plugin in PyMOL. Blue denotes a positively charged surface; red denotes a negatively charged surface. The bound test molecules are shown as green stick models. The 3D images were visualized and rendered in PyMol v2.1.0.[21]

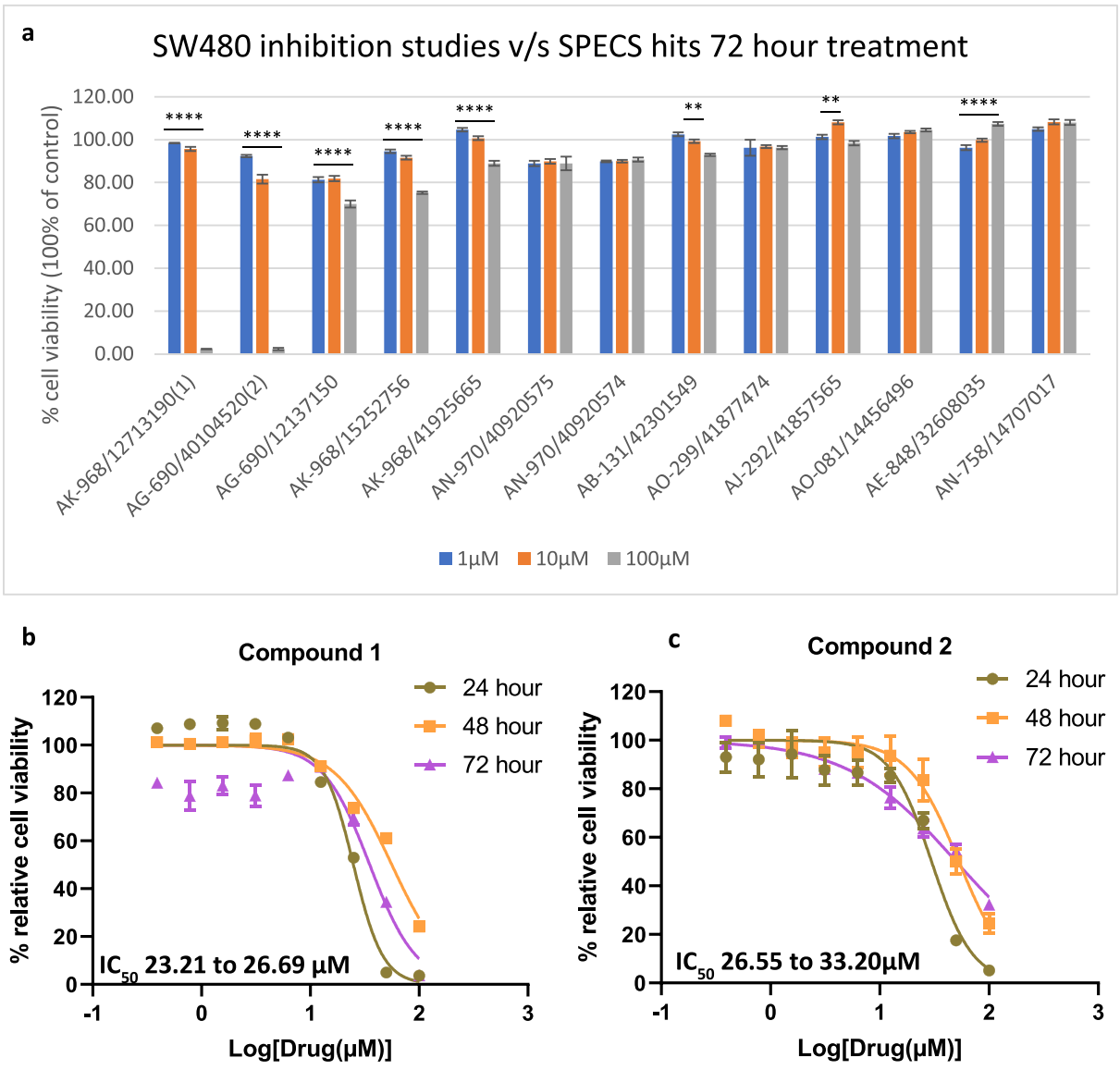

Fig. 3. a) Cytotoxicity assay of test compounds in SW480 cells which express GPR120 at three concentrations 100, 10 and 1 μM. Results from six replicates are expressed as the mean ± Standard error. The cytotoxicity of b) Compound **1** (experimental 24 h IC_{50} 23.21 to 26.69 μM) and; c) Compound **2** (experimental 24 h IC_{50} 26.55 to 33.2 μM) was assayed by using SW480 cells using 9 serial dilutions from 100 μM to 0.39 μM at three different treatment time periods. Results show mean and standard error of 5 replica samples. Results are representative of three individual experiments. Where no error bars are visible, they are obscured by the symbol. Percent relative cell viability for all treatments were quantified and normalised to the maximal response induced by vehicle control. Data for (a) was analysed by two-way ANOVA and asterisk values denote significant differences between 100, 10 and 1 μM treatment for each compound (*$P < 0.05$; **$P < 0.01$; ***$P < 0.001$; ****$P < 0.0001$).

positive charge should be able to enter the binding tunnel without facing any resistance from the neutral or weakly charged residues at the opening.[38] Once the ligand enters the pocket the strong attractive charges should stabilise the protein–ligand binding, playing an important role in the binding kinetics. Steered molecular dynamics (SMD) studies can be insightful to further probe the binding kinetics of ligands w.r.t the charged surfaces of binding tunnel.[38,39]

In vitro cytotoxicity assay

The selected 13 compounds from the *in silico* VS were evaluated for their potential anticancer activity by an alamar blue cytotoxicity assay (see methods) using SW480 cells expressing GPR120.[6] For initial screening, the SW480 cell-line was treated with three concentrations (100, 10 and 1 μM) of each test compound for 72 h. As illustrated in Fig 3a, most of the compounds (11 out of 13) displayed null to negligible (~30%) cytotoxicity against SW480 cells at the highest tested concentration of 100 μM. However, two of the test compounds showed significant (>90%) inhibitory effects on cell growth with micromolar affinities (at 100 μM), reported in Fig 3a.

The two active compounds - AK-968/12713190 (compound **1**) and AG-690/40104520 (compound **2**), were further tested at a wider concentration panel to construct a dose–response curve and determine their IC_{50} values (see Fig 3b, c). Both the test compounds were active in cell line measurements with modest inhibitory activity at different treatment times. The 24 h drug treatments indicated IC_{50} value of 23.21–26.69 μM for **1** and 26.55–33.2 μM for **2**.

As the Dose-response-time (DRT) can highlight the dose–response patterns over time in pharmacological studies,[40] these two test compounds were tested over a longer treatment times of 48 h and 72 h for

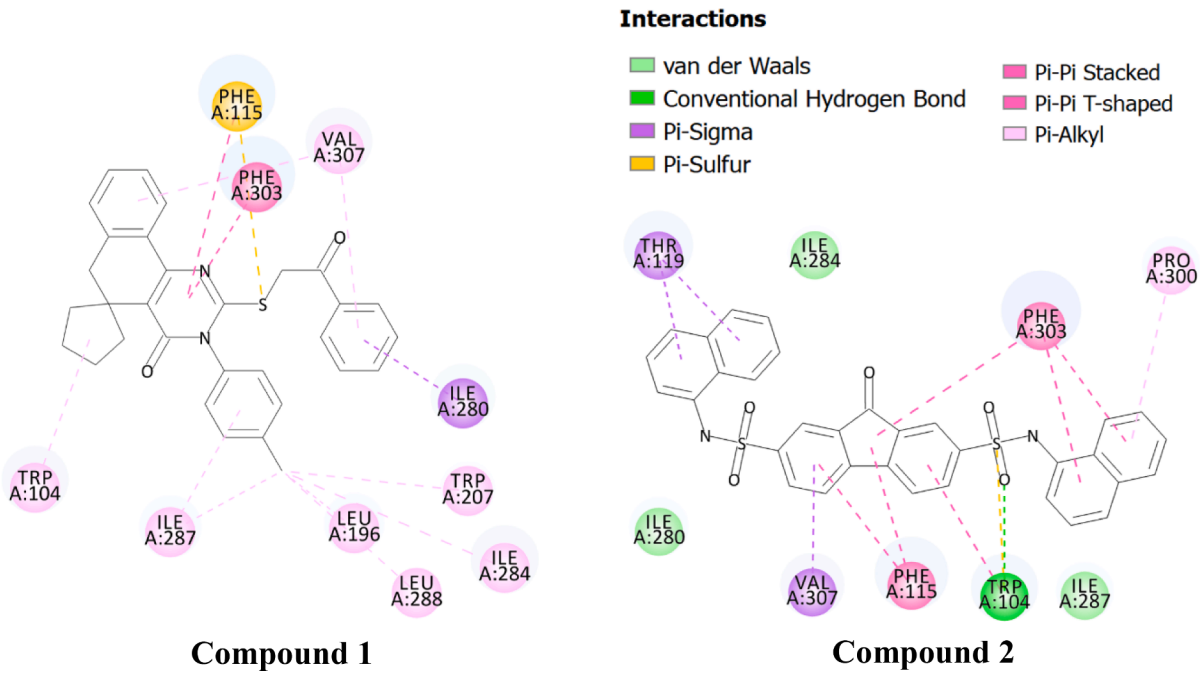

Fig. 4. 2D interaction maps of docked poses of compounds **1** and **2**. The 2D interaction maps were generated in BIOVIA DS Client visualizer 2019.[22]

their cytotoxicity activity (see Fig 3b, c). After 48 h, the IC_{50} of both compounds drops to ~50–60 μM. Similar effects over time have been reported in another oncogenic study[41] suggesting that the cells might have developed acquired resistance to test compounds at lower concentration after 48 h of exposure. This acquired resistance might enable them to escape the cytostatic state and start cell proliferation which can be traced back to the augmented chemoresistance in breast cancer treatment through GPR120 overexpression.[7] Also, the increased metabolic activity of cancer cells can be related to anticancer drug metabolism responsible for the resistance to cytotoxic agents,[42,43] hence reducing the cytotoxicity of these two compounds over time. While the 72 h experiments showed a slight decrease of 10 μM in IC_{50} values of both compounds, it should be noted that the drug concentrations were not replaced over the treatment time intervals. The decreased cell growth or increased cytotoxic effects of these two compounds at 72 h might be the result of a lack of nutrients and increased metabolic waste in the culture solution.[44,45]

SAR/similarity search and in vitro screening of SAR compounds

The top-scoring docked poses of compounds **1** and **2** (see Fig 4) predicted that the two molecules interact with a number of residues reported significant for protein-ligand binding by Hudson et al 2014[30] and which also interacted with the selected docked pose of TUG891 (see Fig 1) such as Ile280, Ile284, Val307. Compound **1** consists of a benzoquinazoline ring structure as the chemical scaffold with smaller benzylmethyl and benzyl substituents. The phenylalanine residue at TM3 (Phe115) shows strong π-π interactions with the main scaffold as well as π-sulfur interactions with the sulfanyl linker (see Fig 4). While compound **2** consists of a 9-fluorenone as the chemical scaffold with

Table 2
SAR of Compound **1** with modified groups to determine functional potency.

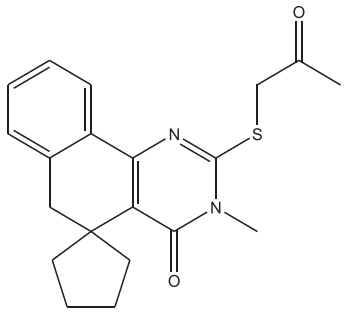

Compound **1** substructure

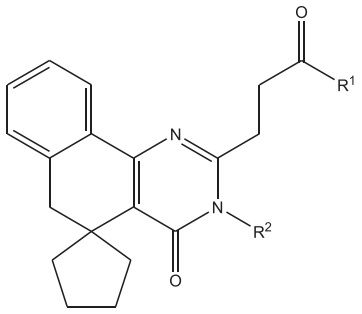

Generic chemical formula

	SPECS Compound ID	-R^1	-R^2	Docking Cscore	Experimental IC_{50} (μM)	Lipinski's Violations
3	**AL-281/36997030**	-C_6H_4Cl	–CH_3	−9.339	22.92 to 27.58	0
4	**AJ-292/12930007**	-C_6H_4Cl	-C_5H_9	−9.741	24.26 to 26.95	2 (MW 505; logP 4.57)
5	**AL-281/36997031**	-C_6H_4Cl	-C_6H_5	−10.706	5.890 to 6.715	2 (MW 513; logP 4.03)
6	**AG-690/12134207**	-C_6H_4Cl	-C_2H_4-C_6H_5	−10.213	68.92 to 84.21	2 (MW 541; logP 4.32)
7	**AL-281/36997034**	-C_6H_4Cl	-C_6H_4-O- CH_3	−9.668	6.789 to 7.502	2 (MW 543; logP 4.38)
8	**AN-512/12673388**	-C_6H_4Br	-C_6H_4-CH_3	−10.704	25.54 to 28.87	2 (MW 571; logP 4.77)
9	**AN-512/12674229**	-C_6H_4Br	2,2-$(CH_3)_2$-C_5H_7O	−9.988	N/A	2 (MW 593; logP 4.5)

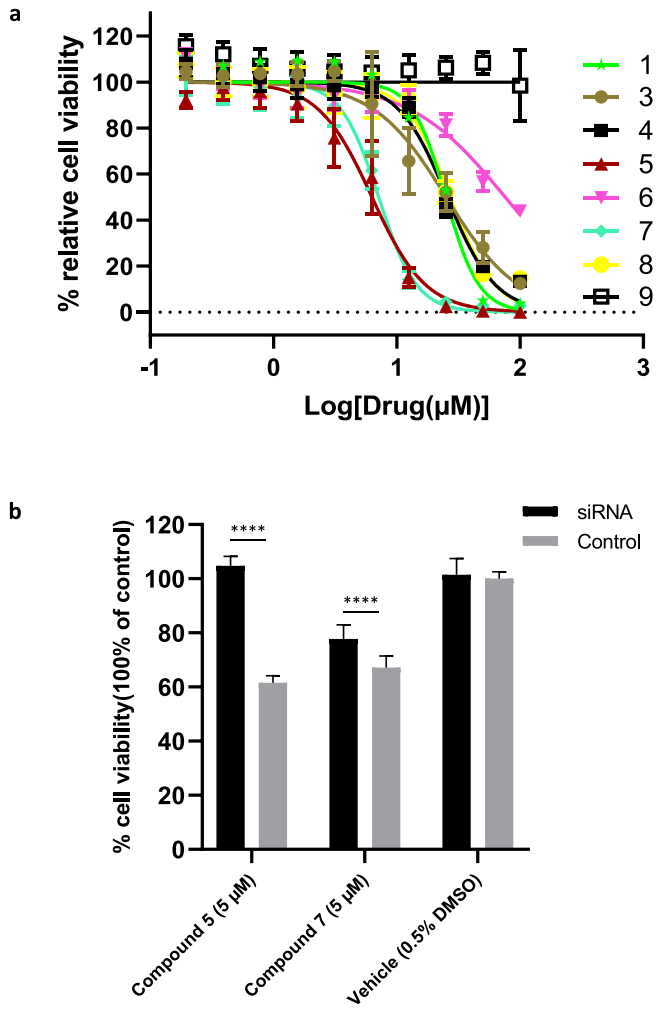

Fig. 5. a) Cytotoxicity profile of compound **1** SAR analogues using SW480 cells for 24-hour treatment. Results show mean and standard error of 4 replica samples. Where no error bars are visible, they are obscured by the symbol; b) siRNA-mediated silencing of GPR120 in SW480 cells – Compound **5** and **7** were screened against GPR120-siRNA and scrambled-siRNA (control) transfected SW480 cells. Results from five replicates are expressed as the mean ± standard error, ****p < 0.0001 as indicated (ANOVA, Tukey's multiple comparisons test). Percent relative cell viability for all treatments were quantified and normalised to the maximal response induced by vehicle control.

symmetric dimeric naphthalene groups at both ends linked by an aminosulfonyl. The presence of dimeric naphthyl substituents showing strong hydrophobic π-π stacked interactions at one end and simple π-Sigma interactions at the other suggesting strong binding interactions in the binding pocket.

The chemical scaffold of **2** is 9-fluorenone (PubChem CID: 10241) which is actively used in preparation of antimalarial drugs, functional polymers, and dyes.[46] Of the two selected compounds, **1** was prioritized based on the strong docking predictions with the GPR120S model, its novelty with respect to the literature and the micromolar cytotoxic activity in CRC cell line, for SAR studies. To expand the SAR profile, the generic chemical structure, *dihydrospiro(benzo[h]quinazoline-5,1′-cyclopentane)-4(3H)-one*, in combination with sulfanyl acetone tail was used as query for substructure search against the pre-processed SPECS database using DS pipeline pilot (Table 2).

The substructure search resulted in 16 compounds from the pre-screened SPECS database. This set of compounds explored R-groups in position R^1 and R^2 of the scaffold (see Table 2) in combination with in silico ADME profiling using SwissADME (http://www.swissadme.ch/)[47] to procure the selective compounds for *in vitro* screening. The analogues were selected exploring the alkyl to aryl substitutions at the R^2 position and simple halobenzene susbstitutions at the R^1 position connected by a sulfanyl acetone linker keeping *dihydrospiro(benzo[h]quinazoline-5,1′-cyclopentane)-4(3H)-one* scaffold structure intact. Based on the docking analysis, manual screening and the availability of compounds at SPECS, seven compounds were tested for *in vitro* cytotoxicity assay in SW480 cell line as discussed above (see Fig 5a).

Based on the SAR study, the IC_{50} values of the new hits enable an initial identification of the essential pharmacophore features required in the *dihydrospiro(benzo[h]quinazoline-5,1′-cyclopentane)-4(3H)-one* scaffold. The presence of an aromatic halogen at the sulfanyl acetone tail exhibited an increase in potency (**3**, **5**, **7**). However, the substitution of chloride in comparison to bromide seems to be more effective for pharmacological activity. The drop in potency of **8** w.r.t the parent compound (1) and **5** can be related to larger atomic size of bromine atom compared to chlorine which can result in decreased solubility and hence lowering the bioavailability of the compounds. Although not predicted in molecular docking which showed similar binding scores −10.22, −10.706 and −10.704 (compounds **1**, **5** and **8** respectively), the greater size of bromine might be responsible for steric clashes with neighbouring residues in the binding pocket which can be further analysed by future MD studies. Incorporation of fluoroaromatics at the sulfanyl acetone tail may increase the solubility and hence bioavailability of these SAR analogues as the fluorine atom is smaller in size and also exhibit slight electronegativity which can increase the electrostatic bonding affinity of the compounds.

Substitution of the benzo-methyl at the R^2 position in the parent structure and **8** by a smaller methyl group (**3**) or an aromatic six-membered group (**5**) resulted in a significant increase in potency of the analogues. The substitution of a non-aromatic cyclic group (**4**) resulted in reduced activity of the parent compound (1). The addition of a methoxy group to this aromatic ring at R^2 position in **7** resulted in the second most active compound of the SAR profiling. The quinazoline ring linked to five or six membered aromatic ring structure at R^2 position by a single C—C bond length seems to be the optimum as when the linker length in **5** is increase (-C-$\mathbf{C_2H_4}$-C-), the cytotoxic activity of **6** registered a drastic decrease from ~ 6 μM to ~ 80 μM. The total inactivity of **9** may confirm the above inferences as it contains bromo-aromatic group at R^1 position and non-aromatic cyclic ring with a longer linker at the R^2 position.

SAR analysis is a state-of-the-art and precise method to explore bioactive analogues of an active compound which may improve binding affinity to a protein target.[19,20] Of the present SAR study, analogues (**5** and **7**) exhibited the best cytotoxic activity. When both these compounds were tested at 5 μM (below experimental IC_{50}) in GPR120-silenced SW480 cells, this cytotoxic effect of 5 was significantly suppressed in GPR120-siRNA transfected SW480 cells (Fig 5b) while **7** showed ~10% higher cytotoxicity levels in siRNA transfected cells. The comparative study between GPR120-silenced and control experiments suggested that **5** exhibited cytotoxic effects through GPR120 binding while cytotoxic activity of **7** might be through multiple targets including GPR120. However, further *in silico* and *in vitro* validation is required to confirm their anti-cancer potential targeting GPR120. As literature suggests that high levels of GPR120 expression in CRC cell lines increases the cell proliferation rate and reduces apoptosis,[6] it can be hypothesized that compound 5 and 7 inhibit GPR120 and hence increase the apoptosis rate. A comparative study of these test compounds against a competitive antagonist would be useful, but as mentioned earlier no GPR120 antagonists are available to date. AH7614 (4-Methyl-N-9H-xanthen-9-yl-benzenesulfonamide) was first reported as a GPR120 selective antagonist by GlaxoSmithKline in 2014[48] but its mechanism of antagonism was not known. Later collaborative research by the Ulven and Milligan labs in 2017[49] reported that AH7614 was a negative allosteric modulator of GPR120.

In summary, with the identification of the two most active analogues

from the SAR profiling of parent compound **1** (AK-968/12713190) with a *dihydrospiro(benzo[h]quinazoline-5,1′-cyclopentane)-4(3H)-one* scaffold, our study has successfully identified a novel scaffold for developing potential therapeutics for CRC management. The main scaffold can be further enhanced focusing on the substitution and addition of key structural groups as mentioned in the SAR study. Future studies will confirm the role of GPR120 in the cytotoxic activity exhibited by these compounds.

Funding

Fiosraigh Dean of Graduate Research School Award (2016–2020) for Ajay Pal; Grant No. PB04185.

Ethics approval

Not applicable.

Consent to participate

Not applicable.

Consent for publication

The authors hereby give consent for the publication of this manuscript.

Availability of data and material

Supplementary material has been provided.

Code availability

Not applicable.

Authors' contributions

Research design AJ, JC, GK; Experimental work AJ; Data analysis AJ, JC, GK; Manuscript preparation AJ; Manuscript revision AJ, JC, GK.

Declaration of Competing Interest

The authors declare that they have no known competing financial interests or personal relationships that could have appeared to influence the work reported in this paper.

Acknowledgments

The authors gratefully acknowledge Technological University Dublin (TU Dublin) for providing financial assistance through Fiosraigh Dean of Graduate Research School Award doctoral fellowship (Grant No. PB04185). The authors wish to acknowledge the Irish Centre for High-End Computing (ICHEC) for the provision of computational facilities and support.

Appendix A. Supplementary data

Supplementary data to this article can be found online at https://doi.org/10.1016/j.bmcl.2020.127672.

References

1 Galindo M, Voigt N, Stein J, et al. G protein-coupled receptors in human fat taste perception. *Chem Senses*. 2011;37:123–139. https://doi.org/10.1093/chemse/bjr069.
2 Hirasawa A, Tsumaya K, Awaji T, et al. Free fatty acids regulate gut incretin glucagon-like peptide-1 secretion through GPR120. *Nat Med*. 2004;11:90–94. https://doi.org/10.1038/nm1168.
3 Davenport A, Alexander S, Sharman J, Pawson A, Benson H, Monaghan A. International union of basic and clinical pharmacology. LXXXVIII. G protein-coupled receptor list: recommendations for new pairings with cognate ligands. *Pharmacol Rev*. 2013;65:967–986. https://doi.org/10.1124/pr.112.007179.
4 Fredriksson R, Höglund P, Gloriam D, Lagerström M, Schiöth H. Seven evolutionarily conserved human rhodopsin G protein-coupled receptors lacking close relatives. *FEBS Lett*. 2003;554:381–388. https://doi.org/10.1016/s0014-5793(03)01196-7.
5 Hirasawa A, Hara T, Katsuma S, Adachi T, Tsujimoto G. Free fatty acid receptors and drug discovery. *Biol Pharm Bull*. 2008;31:1847–1851. https://doi.org/10.1248/bpb.31.1847.
6 Wu Q, Wang H, Zhao X, et al. Identification of G-protein-coupled receptor 120 as a tumor-promoting receptor that induces angiogenesis and migration in human colorectal carcinoma. *Oncogene*. 2013;32:5541–5550. https://doi.org/10.1038/onc.2013.264.
7 Wang X, He S, Gu Y, et al. Fatty acid receptor GPR120 promotes breast cancer chemoresistance by upregulating ABC transporters expression and fatty acid synthesis. *Ebiomedicine*. 2019;40:251–262. https://doi.org/10.1016/j.ebiom.2018.12.037.
8 Senatorov I, Moniri N. The role of free-fatty acid receptor-4 (FFA4) in human cancers and cancer cell lines. *Biochem Pharmacol*. 2018;150:170–180. https://doi.org/10.1016/j.bcp.2018.02.011.
9 Folkman J. Angiogenesis: an organizing principle for drug discovery? *Nat Rev Drug Discovery*. 2007;6:273–286. https://doi.org/10.1038/nrd2115.
10 Yadav L. Tumour angiogenesis and angiogenic inhibitors: a review. *J Clin Diagnost Res*. 2015. https://doi.org/10.7860/jcdr/2015/12016.6135.
11 Shimpukade B, Hudson B, Hovgaard C, Milligan G, Ulven T. Discovery of a potent and selective GPR120 agonist. *J Med Chem*. 2012;55:4511–4515. https://doi.org/10.1021/jm300215x.
12 Deshpande N. The RCSB protein data bank: a redesigned query system and relational database based on the mmCIF schema. *Nucleic Acids Res*. 2004;33:D233–D237. https://doi.org/10.1093/nar/gki057.
13 Akhtar N, Jabeen I, Jalal N, Antilla J. Structure-based pharmacophore models to probe anticancer activity of inhibitors of protein kinase B-beta (PKB β). *Chem Biol Drug Des*. 2018;93:325–336. https://doi.org/10.1111/cbdd.13418.
14 Ganesan A, Barakat K. Applications of computer-aided approaches in the development of hepatitis C antiviral agents. *Expert Opin Drug Discov*. 2017;12:407–425. https://doi.org/10.1080/17460441.2017.1291628.
15 Li Q. Virtual screening of small-molecule libraries, Small Molecule. *Drug Discovery*. 2020:103–125. https://doi.org/10.1016/b978-0-12-818349-6.00004-2.
16 Wang Z, Sun H, Shen C, et al. Combined strategies in structure-based virtual screening. *PCCP*. 2020;22:3149–3159. https://doi.org/10.1039/c9cp06303j.
17 Basith S, Cui M, Macalino S, et al. Exploring G protein-coupled receptors (GPCRs) ligand space via cheminformatics approaches: impact on rational drug design. *Front Pharmacol*. 2018;9. https://doi.org/10.3389/fphar.2018.00128.
18 Clark D. What has virtual screening ever done for drug discovery? *Expert Opin Drug Discov*. 2008;3:841–851. https://doi.org/10.1517/17460441.3.8.841.
19 Jaakola V, IJzerman A. The crystallographic structure of the human adenosine A2A receptor in a high-affinity antagonist-bound state: implications for GPCR drug screening and design. *Curr Opin Struct Biol*. 2010;20:401–414. https://doi.org/10.1016/j.sbi.2010.05.002.
20 Ma Y, Wang S, Xu W, Wang R, Chou K. Design novel dual agonists for treating type-2 diabetes by targeting peroxisome proliferator-activated receptors with core hopping approach. *PLoS ONE*. 2012;7, e38546. https://doi.org/10.1371/journal.pone.0038546.
21 W.L. DeLano, The PyMol Molecular Graphics System, Schrödinger, LLC. Version 2.1.0. https://github.com/schrodinger/pymol-open-source.
22 Dassault Systèmes BIOVIA. *Discovery Studio Modeling Environment, Release 2017*. San Diego: Dassault Systèmes; 2016.
23 Webb B, Sali A. Comparative protein structure modeling using MODELLER. *Curr Protoc Protein Sci*. 2016;86. https://doi.org/10.1002/cpps.20.
24 Berthold M, Cebron N, Dill F, et al. KNIME - the Konstanz information miner. *ACM SIGKDD Explorations Newsletter*. 2009;11:26–31. https://doi.org/10.1145/1656274.1656280.
25 Krivov G, Shapovalov M, Dunbrack R. Improved prediction of protein side-chain conformations with SCWRL4. *Proteins Struct Funct Bioinf*. 2009;77:778–795. https://doi.org/10.1002/prot.22488.
26 Chen V, Arendall W, Headd J, et al. MolProbity: all-atom structure validation for macromolecular crystallography. *Acta Crystallogr D Biol Crystallogr*. 2009;66:12–21. https://doi.org/10.1107/s0907444909042073.
27 Laskowski R, MacArthur M, Moss D, Thornton J. PROCHECK: a program to check the stereochemical quality of protein structures. *J Appl Crystallogr*. 1993;26:283–291. https://doi.org/10.1107/s0021889892009944.
28 Morris G, Huey R, Lindstrom W, et al. AUTODOCK4 and Autodocktools4: automated docking with selective receptor flexibility. *J Comput Chem*. 2009;30:2785–2791. https://doi.org/10.1002/jcc.21256.
29 Koes D, Baumgartner M. Camacho c. Lessons Learned in Empirical Scoring with smina from the CSAR 2011 Benchmarking Exercise. *J Chem Inf Model*. 2013;53:1893–1904. https://doi.org/10.1021/ci300604z.
30 Hudson B, Shimpukade B, Milligan G, Ulven T. The molecular basis of ligand interaction at free fatty acid receptor 4 (FFA4/GPR120). *J Biol Chem*. 2014;289:20345–20358. https://doi.org/10.1074/jbc.m114.561449.
31 Hudson B, Shimpukade B, Mackenzie A, et al. The pharmacology of TUG-891, a potent and selective agonist of the free fatty acid receptor 4 (FFA4/GPR120),

demonstrates both potential opportunity and possible challenges to therapeutic agonism. *Mol Pharmacol*. 2013;84:710–725. https://doi.org/10.1124/mol.113.087783.
32 Trott O, Olson A. AutoDock Vina: Improving the speed and accuracy of docking with a new scoring function, efficient optimization, and multithreading. *J Comput Chem*. 2009:NA-NA. https://doi.org/10.1002/jcc.21334.
33 Durrant J, McCammon J. NNScore 2.0: a neural-network receptor-ligand scoring function. *J Chem Inform Model*. 2011;51:2897–2903. https://doi.org/10.1021/ci2003889.
34 Karney C, Ferrara J, Brunner S. Method for computing protein binding affinity. *J Comput Chem*. 2004;26:243–251. https://doi.org/10.1002/jcc.20167.
35 Sun Q, Hirasawa A, Hara T, et al. Structure-activity relationships of GPR120 agonists based on a docking simulation. *Mol Pharmacol*. 2010;78:804–810. https://doi.org/10.1124/mol.110.066324.
36 Watson S, Brown A, Holliday N. Differential signaling by splice variants of the human free fatty acid receptor GPR120. *Mol Pharmacol*. 2012;81:631–642. https://doi.org/10.1124/mol.111.077388.
37 Salentin S, Schreiber S, Haupt V, Adasme M, Schroeder M. PLIP: fully automated protein–ligand interaction profiler. *Nucleic Acids Res*. 2015;43:W443–W447. https://doi.org/10.1093/nar/gkv315.
38 Shen J, Li W, Liu G, Tang Y, Jiang H. Computational insights into the mechanism of ligand unbinding and selectivity of estrogen receptors. *J Phys Chem B*. 2009;113:10436–10444. https://doi.org/10.1021/jp903785h.
39 Wong C. Steered molecular dynamics simulations for uncovering the molecular mechanisms of drug dissociation and for drug screening: a test on the focal adhesion kinase. *J Comput Chem*. 2018;39:1307–1318. https://doi.org/10.1002/jcc.25201.
40 Gabrielsson J, Andersson R, Jirstrand M, Hjorth S. Dose-response-time data analysis: an underexploited trinity. *Pharmacol Rev*. 2018;71:89–122. https://doi.org/10.1124/pr.118.015750.
41 Zakharia Y, Monga V, Swami U, et al. Targeting epigenetics for treatment of BRAF mutated metastatic melanoma with decitabine in combination with vemurafenib: a phase lb study. *Oncotarget*. 2017;8:89182–89193. https://doi.org/10.18632/oncotarget.21269.
42 Cree IA. Cancer biology. *Methods Mol Biol*. 2011;731:1–11. https://doi.org/10.1007/978-1-61779-080-5_1.
43 Iyanagi T. Molecular mechanism of phase I and phase II drug metabolizing enzymes: implications for detoxification. *Int Rev Cytol*. 2007:35–112. https://doi.org/10.1016/s0074-7696(06)60002-8.
44 Ackermann T, Tardito S. Cell culture medium formulation and its implications in cancer metabolism. *Trends Cancer*. 2019;5:329–332. https://doi.org/10.1016/j.trecan.2019.05.004.
45 Ackermann T, Tardito S. Cell Culture Medium Formulation and Its Implications in Cancer Metabolism. *Trends Cancer*. 2019 Jun;5(6):329–332. https://doi.org/10.1016/j.trecan.2019.05.004.
46 9-Fluorenone, Pubchem.Ncbi.Nlm.Nih.Gov. (2020). https://pubchem.ncbi.nlm.nih.gov/compound/9-Fluorenone (accessed 10 May 2020).
47 Daina A, Michielin O, Zoete V. SwissADME: a free web tool to evaluate pharmacokinetics, drug-likeness and medicinal chemistry friendliness of small molecules. *Sci Rep*. 2017;7. https://doi.org/10.1038/srep42717.
48 Sparks S, Chen G, Collins J, et al. Identification of diarylsulfonamides as agonists of the free fatty acid receptor 4 (FFA4/GPR120). *Bioorg Med Chem Lett*. 2014;24:3100–3103. https://doi.org/10.1016/j.bmcl.2014.05.012.
49 Watterson K, Hansen S, Hudson B, et al. Probe-dependent negative allosteric modulators of the long-chain free fatty acid receptor FFA4. *Mol Pharmacol*. 2017;91:630–641. https://doi.org/10.1124/mol.116.107821.